Research in Astronomy and Astrophysics, 23:045008 (9pp), 2023 April https://doi.org/10.1088/1674-4527/acc150

Study of Central Intensity Ratio of Seyfert Galaxies in Nearby Universe

K. T. Vinod[1], C. Baheeja[1], S. Aswathy[2], and C. D. Ravikumar[1]
[1] Department of Physics, University of Calicut, Malappuram-673635, India; vinod2085@gmail.com
[2] Department of Physics, Providence Women's College, Calicut-673009, India
Received 2022 September 22; revised 2023 January 21; accepted 2023 February 20; published 2023 March 24

Abstract

We use the recently discovered simple photometric parameter Central Intensity Ratio (CIR) determined for a sample of 57 nearby ($z < 0.02$) Seyfert galaxies to explore the central features of galaxies and their possible connection with galaxy evolution. The sample of galaxies shows strong anti-correlation between CIR and mass of their central supermassive black holes (SMBHs). The SMBH masses of ellipticals are systematically higher for a given CIR value than those for lenticulars and spirals in the sample. However, the correlation between CIR and central velocity dispersion is weak. CIR appears less influenced by the excess flux produced by the central engine in these galaxies, when compared to spectroscopic parameters like velocity dispersion and O IV flux, and proves to be a fast and reliable tool for estimating central SMBH mass.

Key words: Galaxy: evolution – galaxies: active – galaxies: photometry – (galaxies:) quasars: supermassive black holes – galaxies: Seyfert

1. Introduction

The central supermassive black hole (SMBH) residing in massive galaxies is believed to play a key role in the evolution scenario of host galaxies. The evolution mechanism of the central engine of every galaxy is connected with the star formation process in the host galaxy. It is commonly accepted that the accretion mechanism is the prime reason for the origin and growth of active galactic nuclei (AGNs) in the nuclear region of galaxies (Kawakatu et al. 2006; Ellison et al. 2011; Silverman et al. 2011; Villforth et al. 2012).

AGNs are hosted at the centers of elliptical galaxies or bulge dominating spheroids across all redshifts (Kauffmann et al. 2003; Pović et al. 2009), whereas the morphology of local Seyfert galaxies is generally spiral (Ho et al. 1995; Ho 2008). Intense circumnuclear star formation plays a crucial role in the evolution and emission process of Seyfert galaxies, specifically, Sy2 galaxies (e.g., Terlevich & Melnick 1985; Cid Fernandes et al. 1995; Maiolino et al. 1998; Cid Fernandes et al. 2001; González Delgado et al. 2001).

Seyfert galaxies are among the most studied objects in the radio quiet (RQ) category, along with quasars (Weedman 1977; Osterbrock & Martel 1993; Rashed et al. 2015). The role of feedback by the central SMBH in the relationships between the mass of the SMBH and bulge properties of Seyfert galaxies is still unclear because the merger events govern the formation of bulges while Seyfert galaxies are believed to be evolving through secular evolution (Hopkins et al. 2006; Kormendy & Ho 2013; Heckman & Best 2014). Recent studies revealed the existence of fast outflows of ionized gas in nearby Seyfert galaxies, but their influence on star formation is still under debate (Christensen et al. 2006; Krause et al. 2007; Wang et al. 2012; García-Burillo et al. 2014; Morganti et al. 2015; Querejeta et al. 2016). However, if the host galaxies possess such outflows, they could expel the gas from the central region and suppress the star formation (Alexander & Hickox 2012; García-Burillo et al. 2014; Alatalo et al. 2015; Hopkins et al. 2016; Wylezalek & Zakamska 2016).

The masses of central SMBHs are reported to correlate well with the stellar mass and stellar velocity dispersion of the bulges of their host galaxies (see, e.g., Magorrian et al. 1998; Ferrarese & Merritt 2000; Gebhardt et al. 2000; Marconi & Hunt 2003; Häring & Rix 2004; Kormendy & Ho 2013; McConnell & Ma 2013; Savorgnan & Graham 2015). The bulges and SMBHs seem to evolve together and regulate each other (Alonso-Herrero et al. 2013). The relations (between $M_{\rm BH}$, bulge mass and stellar velocity dispersion) propose a strong connection between the formation of black hole mass, emergence of AGNs and the host galaxy evolution (Ferrarese & Merritt 2000; Gültekin et al. 2009) as well.

Central light concentration is a vital parameter, which can be used as a tracer of the disk to bulge ratio, star formation activity and galaxy evolution (Abraham et al. 1994; Conselice 2003). The Central Intensity Ratio (CIR), a new photometric parameter, is well correlated with the masses of central SMBHs of the spheroid of early-type galaxies (ETGs, Aswathy & Ravikumar 2018). Furthermore, CIR is an efficient photometric tool to study the central and structural properties of spiral galaxies, especially barred systems, and also gives some valid information regarding nuclear star formation and AGN formalism in host galaxies (Aswathy & Ravikumar 2020). In

Table 1
Table 1 Lists the Properties of Sample Galaxies

Galaxy	Distance (Mpc)	Seyfert Type	Morphology	CIR	ΔCIR	log M_{BH} ($M_\odot$)	Ref	σ (km s^{-1})	O IV Flux (erg cm^{-2} s^{-1})	Log SFR ($M_\odot$ yr^{-1})	ΔSFR	HST Obs.
IC 2560	40.7	S2	(R')SB(r)b	1.44	0.03	6.64	1	136.5	5.43E-013	0.67	0.013	WFPC2_F814
IC 3639	35.3	S2	SB(rs)bc	1.27	0.02	6.83	2	97.1	3.55E-013	1.64	0.040	WFPC2_F606
NGC 0613	20.7	S?	SB(rs)bc	0.86	0.02	7.60	3	122.1	⋯	0.91	0.007	WFPC2_F814
NGC 0788	54.1	S2	SA(s)0/a	1.16	0.03	7.51	2	134.4	1.80E-013	1.01	0.021	WFPC2_F606
NGC 1275	70.1	S2	E-cD	1.07	0.03	8.58	2	244.6	1.85E-013	2.22	0.170	WFPC2_F702
NGC 1358	53.6	S2	SAB(r)0/a	1.17	0.02	7.88	2	215.1	7.61E-014	⋯	⋯	WFPC2_F606
NGC 1365	21.5	S1.8	SB(s)b	1.78	0.03	6.05	4	141.1	1.58E-012	1.06	0.009	WFPC2_F814
NGC 1386	10.6	S2	SB0+(s)	1.10	0.02	7.23	2	133.1	8.70E-013	−0.11	0.001	WFPC2_F814
NGC 1399	19.4	S2	E1 pec	0.58	0.01	8.94	3	332.2	⋯	⋯	⋯	WFPC2_F814
NGC 1433	13.3	S2	(R')SB(r)ab	0.91	0.02	7.24	5	107	6.07E-014	0.38	0.002	WFPC2_F814
NGC 1566	19.4	S1.5	SAB(s)bc	1.03	0.03	7.11	4	97.7	8.88E-014	0.67	0.005	WFPC2_F814
NGC 1667	61.2	S2	SAB(r)c	1.09	0.03	7.88	2	169.4	9.28E-014	1.51	0.049	WFPC2_F606
NGC 1672	16.7	S2	SB(s)b	0.77	0.02	7.70	6	109.5	⋯	1.35	0.010	WFPC2_F814
NGC 1808	12.3	S2	(R)SAB(s)a	0.90	0.02	7.20	7	126.1	⋯	−0.11	0.001	WFPC2_F814
NGC 2273	28.4	S2	SB(r)a	1.15	0.03	7.30	2	141	1.47E-013	0.14	0.004	WFPC2_F791
NGC 2639	42.6	S1.9	(R)SA(r)a	0.69	0.03	7.94	2	175.3	3.27E-014	0.43	0.009	WFPC2_F814
NGC 2782	37	S2	SAB(rs)a pec	1.21	0.03	7.70	8	182.2	⋯	1.81	0.032	WFPC2_F814
NGC 2974	20.9	S2	E4	1.20	0.02	8.23	9	232.2	⋯	⋯	⋯	WFPC2_F814
NGC 3081	34.2	S2	(R)SAB(r)0/a	0.88	0.03	7.20	3	118.8	9.89E-013	⋯	⋯	WFPC2_F814
NGC 3169	17.4	S	SA(s)a pec	0.74	0.02	8.01	10	184.9	⋯	−0.42	0.001	WFPC2_F814
NGC 3185	21.3	S2	(R)SB(r)a	1.58	0.03	6.52	2	76.1	4.70E-014	−0.44	0.001	WFPC2_F814
NGC 3227	20.6	S1.5	SAB(s)a pec	1.66	0.00	6.75	11	126.8	5.71E-013	⋯	⋯	ACS_F814
NGC 3281	44.7	S2	SA(s)ab pec	0.86	0.04	7.28	2	168.6	1.39E-012	⋯	⋯	WFPC2_F606
NGC 3486	7.4	S2	SAB(r)c	1.10	0.03	7.00	12	60.2	3.30E-014	−0.41	0.001	WFPC2_F814
NGC 3489	6.73	S2	SAB0+(rs)	1.34	0.01	6.78	13	104.2	⋯	−0.41	0.001	WFPC2_F814
NGC 3516	38.9	S1.2	(R)SB(s)0	1.45	0.02	7.23	24	153.6	5.60E-013	1.83	0.037	WFPC2_F791
NGC 3982	17	S1.9	SAB(r)b	1.12	0.03	7.20	14	71.8	1.18E-013	⋯	⋯	WFPC2_F814
NGC 4168	16.8	S1.9	E2	0.74	0.04	9.01	15	182	1.39E-014	⋯	⋯	WFPC2_F702
NGC 4235	35.1	S1.2	SA(s)a	0.99	0.03	7.64	2	133.6	4.33E-014	−0.17	0.003	WFPC2_F606
NGC 4258	8	S1.9	SAB(s)bc	0.72	0.08	7.58	2	132.8	7.49E-014	0.25	0.001	ACS_F814
NGC 4303	13.6	S2	SAB(rs)bc	1.69	0.01	6.58	16	95.1	⋯	⋯	⋯	WFPC2_F814
NGC 4374	18.5	S2	E1	0.60	0.01	8.97	1	277.6	⋯	⋯	⋯	WFPC2_F814
NGC 4472	17.1	S2	E2	0.53	0.02	9.18	17	282	6.64E-014	⋯	⋯	WFPC2_F814
NGC 4477	16.8	S2	SB0(s)	0.79	0.02	7.91	2	172.5	1.69E-014	0.08	0.002	WFPC2_F606
NGC 4501	16.8	S2	SA(rs)b	1.22	0.02	7.30	3	166.2	3.98E-014	0.02	0.004	WFPC2_F606
NGC 4507	59.6	S2	(R')SAB(rs)b	1.34	0.02	7.58	2	149	3.31E-013	⋯	⋯	WFPC2_F814
NGC 4552	15.4	S2	E0-1	0.91	0.01	8.63	18	250.3	⋯	⋯	⋯	WFPC2_F814
NGC 4579	16.8	S1.9	SAB(rs)b	1.13	0.02	7.70	19	165.8	2.83E-014	0.22	0.004	WFPC2_F791
NGC 4594	20	S1.9	SA(s)a	0.91	0.01	8.76	2	225.7	2.62E-014	0.38	0.003	WFPC2_F814
NGC 4698	16.8	S2	SA(s)ab	1.03	0.02	7.61	2	137.4	2.03E-014	−0.53	0.001	WFPC2_F814
NGC 4725	12.4	S2	SAB(r)ab pec	0.87	0.01	7.51	2	131.5	1.24E-014	−0.01	0.002	WFPC2_F606
NGC 5005	21.3	S2	SAB(rs)bc	0.60	0.00	7.84	20	171.5	1.99E-014	1.91	0.013	ACS_F814
NGC 5033	18.7	S1.9	SA(s)c	0.96	0.02	7.64	2	133.9	1.59E-013	−0.28	0.001	WFPC2_F814
NGC 5135	57.7	S2	SB(s)ab	1.11	0.02	7.34	2	125.5	5.83E-013	1.95	0.069	WFPC2_F606
NGC 5194	8.4	S2	SA(s)bc pec	1.27	0.02	6.95	2	87.9	2.46E-013	−0.62	0.000	WFPC2_F814
NGC 5273	21.3	S1.5	SA0(s)	1.47	0.03	6.61	3	65.9	3.72E-014	−0.10	0.001	WFPC2_F791
NGC 5322	24.3	S	E3-4	0.96	0.02	8.51	21	230	⋯	⋯	⋯	WFPC2_F814
NGC 5427	40.4	S2	SA(s)c pec	1.16	0.03	7.58	3	69.9	2.68E-014	1.00	0.013	WFPC2_F606
NGC 5643	14.4	S2	SAB(rs)c	1.45	0.02	6.44	22	⋯	8.16E-013	⋯	⋯	WFPC2_F814
NGC 5806	27.4	S2	SAB(s)b	1.10	0.03	7.07	23	124.3	⋯	⋯	⋯	WFPC2_F814
NGC 6814	25.6	S1.5	SAB(rs)bc	1.29	0.03	7.26	2	108.1	2.13E-013	1.55	0.025	WFPC2_F606
NGC 6951	24.1	S2	SAB(rs)bc	0.73	0.02	7.34	2	114.8	8.37E-014	0.60	0.014	WFPC2_F814
NGC 7469	67	S1.2	(R')SAB(rs)a	1.06	0.00	7.08	2	132.9	3.67E-013	2.99	0.281	ACS_F814

Table 1
(Continued)

Galaxy	Distance (Mpc)	Seyfert Type	Morphology	CIR	ΔCIR	log M_{BH} ($M_\odot$)	Ref	σ (km s^{-1})	O IV Flux (erg cm^{-2} s^{-1})	Log SFR ($M_\odot$ yr^{-1})	ΔSFR	HST Obs.
NGC 7479	32.4	S1.9	SB(s)c	0.85	0.04	7.68	2	151.3	2.67E-013	⋯	⋯	WFPC2_F814
NGC 7582	22	S2	(R')SB(s)ab	1.84	0.02	7.74	2	118.4	2.22E-012	−0.10	0.002	WFPC2_F606
NGC 7590	22	S2	SA(rs)bc	1.09	0.02	6.79	2	91.5	6.88E-014	0.52	0.005	WFPC2_F606
NGC 7743	24.4	S2	(R)SB0+(s)	1.49	0.02	6.72	2	83.5	3.30E-014	⋯	⋯	WFPC2_F606

Note. Name of the galaxy (column 1), Distance (2), Seyfert type (3), Morphology (4), CIR computed in the corresponding filter (5), uncertainty of CIR (6), SMBH mass (7) and corresponding references (8), stellar velocity dispersion adopted from Hyperleda (9), O IV flux taken from Diamond-Stanic et al. (2009) (10), estimated circumnuclear SFR (11), uncertainty of SFR (12), and HST observation (13). References: (1) Kormendy & Ho (2013); (2) Diamond-Stanic & Rieke (2012); (3) van den Bosch (2016); (4) Davis et al. (2014); (5) Smajić et al. (2014); (6) Combes et al. (2019); (7) Busch et al. (2017); (8) Dong & De Robertis (2006); (9) Savorgnan & Graham (2016); (10) Dong & Wu (2015); (11) Onken et al. (2003); (12) Koliopanos et al. (2017); (13) Nowak et al. (2010); (14) Beifiori et al. (2012); (15) Magorrian et al. (1998); (16) Davis et al. (2018); (17) Graham & Soria (2019); (18) Pellegrini (2010); (19) Barth et al. (2001); (20) Izumi et al. (2016); (21) Dullo et al. (2018); (22) Goulding et al. (2010); (23) Dumas et al. (2007).

this light, we perform an optical analysis by utilizing the parameter, CIR, to study the central properties and evolution of Seyfert galaxies.

This paper is organized as follows; Section 2 describes the properties of the sample galaxies and the data reduction techniques employed in this study, and Section 3 deals with results consisting of various correlations. Discussions and conclusions are provided in Section 4.

Throughout this paper, we have used the cosmological parameters: $H_0 = 73.0\,\mathrm{km\,s^{-1}Mpc^{-1}}$; $\Omega_{\mathrm{matter}} = 0.27$; $\Omega_{\mathrm{vacuum}} = 0.73$.

2. The Data and Data Reduction

For this work, we consider a complete sample of Seyfert galaxies drawn from the Revised Shapley-Ames (RSA) catalog (Shapley & Ames 1932; Sandage & Tammann 1987) analyzed by Diamond-Stanic et al. (2009), Diamond-Stanic & Rieke (2012), which includes 114 nearby ($z < 0.02$) Seyfert galaxies brighter than $B_T = 13.2$. We took archival images of the sample observed by the Hubble Space Telescope (HST) to estimate CIR. Among the 114 galaxies, 83 had HST observations in optical bands. From these, 13 galaxies consisting of bad pixels or defects on their images within the region of the central 3″ were removed from the sample. Also, we excluded 10 small galaxies, in which the size of their images is less than the 3″ aperture, and 3 highly inclined galaxies ($i > 70°$). The final sample consists of 57 Seyfert galaxies comprising 40 spiral, 9 lenticular and 8 elliptical galaxies. We chose galaxy images observed with Wide Field and Planetary Camera 2 (WFPC2). It is already reported that though there exist slight variations among values of CIR estimated from nearby filters, the variations are not strong enough to disrupt the observed correlations involving CIR (Sruthi & Ravikumar 2021). Hence we included observations using all filters of WFPC2 from F606W to F814W, giving preference to the filter in the highest wavelength region available. Further, we added four observations using F814W with Advanced Camera for Surveys to improve the statistics for which no WFPC2 images were available. Since the sample galaxies possess an AGN, we have checked the central region of the sample galaxies by constructing residual images using the ellipse task in IRAF. Many sub -structures like bar, ring and spiral-arms are visible in the residual images, however, no significant optical excess flux could be identified in these galaxies that could affect determination of CIR.

Following Aswathy & Ravikumar (2018), the CIR is determined for the sample galaxies by using the aperture photometry (MAG_APER) technique, which is provided in Source-Extractor (SExtractor, Bertin & Arnouts 1996).

$$\mathrm{CIR} = \frac{I_1}{I_2 - I_1} = \frac{10^{0.4(m_2 - m_1)}}{1 - 10^{0.4(m_2 - m_1)}}, \quad (1)$$

where I_1 and I_2 are the intensities and m_1 and m_2 are the corresponding magnitudes of the light within the inner and outer apertures of radii R_1 and R_2, respectively. The inner radius is chosen such that it is a few times the point spread function (PSF). The outer radius (conventionally $2R_1$) is chosen such that the aperture is lying fairly within the galaxy image. For the sample, we chose the inner and outer radii as 1.″5 and 3″, respectively.

Ultraviolet (UV) observations are vital in providing recent star formation activity in galaxies (e.g., Thilker et al. 2005; Gil de Paz et al. 2005, 2007; Koribalski & López-Sánchez 2009). For the estimation of circumnuclear star formation rate (SFR), we examined far-UV (FUV, 1350–1750 Å) data on the sample galaxies observed by the Galaxy Evolution Explorer (GALEX) mission. We considered an aperture size of 10″ at the center of the image to estimate the circumnuclear SFR following López-Sánchez (2010) using the calibration reported by Salim et al. (2007) which is provided in Table 1.

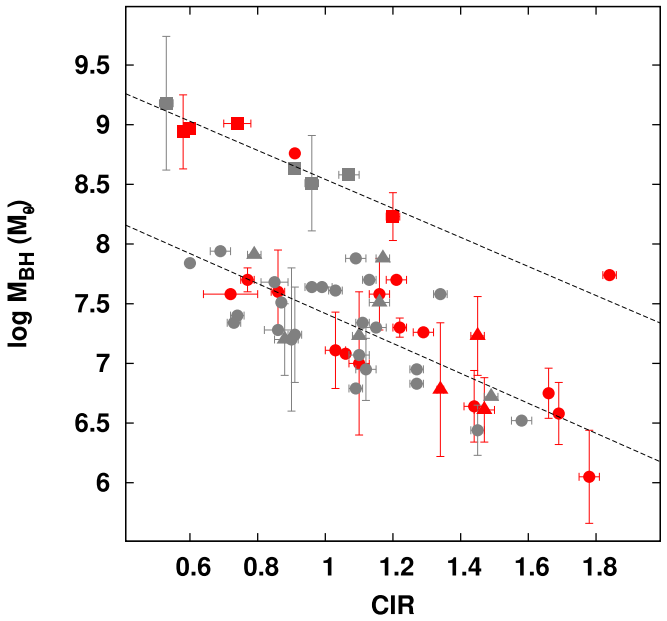

Figure 1. Correlation between the CIR and mass of the SMBH of the sample galaxies. Filled circles, triangles and squares represent spiral, lenticular and elliptical galaxies, respectively. Estimations of masses of SMBHs using dynamical methods are signified as red data points, while gray color is used to represent those from the stellar velocity dispersion measurements of host galaxies.

3. Results

Scaling relations displayed by various structural and dynamical observables of galaxies can shed vital information on formation and evolution processes in galaxies. We have estimated the CIR at the optical centers of 57 Seyfert galaxies observed using HST. The sample properties, along with the estimated values of CIR, are tabulated in Table 1. We next explore various trends involving CIR.

3.1. Variation of CIR with SMBH Mass

The scaling relations of black hole mass are generally determined and explored utilizing the bulge properties of the host galaxies, specifically in ETGs (Kormendy & Richstone 1995; Ferrarese & Merritt 2000; McConnell & Ma 2013). Structural properties of late-type galaxies (LTGs), like the pitch angle of spiral arms, share an intriguing scaling relation with black hole mass (Davis et al. 2018, 2019).

Figure 1 shows the variation of CIR with mass of SMBH for the sample galaxies. Filled circles, triangles and squares represent spiral, lenticular and elliptical galaxies, respectively. We find a strong correlation between the CIR of the Seyfert galaxies and the mass of their central SMBH. However, the ETGs in the sample hosts systematically have high black hole mass when compared to lenticulars and spirals, for the same value of CIR considered. The Pearson's linear correlation coefficient, r, for the correlation exhibited by spirals and lenticulars together is -0.74 with a significance, s, >99.99% (Press et al. 1992) while that for elliptical galaxies is -0.94 with a significance of 99.40%.

Two galaxies, NGC 4594 and NGC 7582, exhibit significant deviation from this correlation. NGC 4594, the Sombrero Galaxy, is reported to have an unusually large bulge mass and a very massive SMBH at the center of the galaxy. It is usually classified as a normal spiral, Sa, galaxy (de Vaucouleurs et al. 1991) but it follows many scaling relations of ellipticals (Gadotti & Sánchez-Janssen 2012). NGC 7582 is reported to host a ring with active star formation within the pc scale radius (≈190 pc) surrounding the nucleus of the galaxy, along with a high stellar velocity dispersion (Riffel et al. 2009). The intense nuclear starburst activity (Cid-Fernandes et al. 2001; Bianchi et al. 2007) can affect its CIR value.

In Section 3.2, we notice that there is no apparent correlation between CIR and stellar velocity dispersion of host galaxies in our sample, even though the latter and mass of SMBH are reported to share a strong correlation. In order to explore this discrepancy, we also employed a color code to distinguish the method adopted to estimate the masses of SMBHs. Masses estimated using a dynamical method (e.g., reverberation mapping, stellar dynamics, maser dynamics and gas dynamics) are shown in red while mass estimations based on stellar velocity dispersion are displayed in gray in Figure 1. If we include only dynamically estimated masses, the correlation coefficient improves to -0.77 at a significance of $s = 99.97\%$, while it reduces drastically to -0.68 ($s = 99.98\%$) when these data points are excluded.

3.2. Variation between the CIR and σ

The variation of CIR with stellar velocity dispersion of the sample galaxies is depicted in Figure 2(a). As already mentioned, there is no significant correlation between CIR and stellar velocity dispersion (σ) of Seyfert galaxies. However, if we exclude the eight ETGs in the sample, the velocity dispersion measurements of galaxies with dynamical estimation of SMBH (red triangles and circles) exhibit larger scatter compared to their gray counterparts. Such a discrepancy is not clear in ETGs. The extreme emission from AGN activity can complicate the measurement of central velocity dispersion in these galaxies (Riffel et al. 2013).

Measurements of stellar velocity dispersion may be biased by the contribution of rotating stellar disks because of the rotational broadening of the stellar absorption lines and the velocity dispersion measurements could be noticeably increased by the rotational effect (Woo et al. 2015). Due to higher velocity-to-dispersion (V/σ) ratios, the rotational effect is significantly more prominent in LTGs than in ETGs.

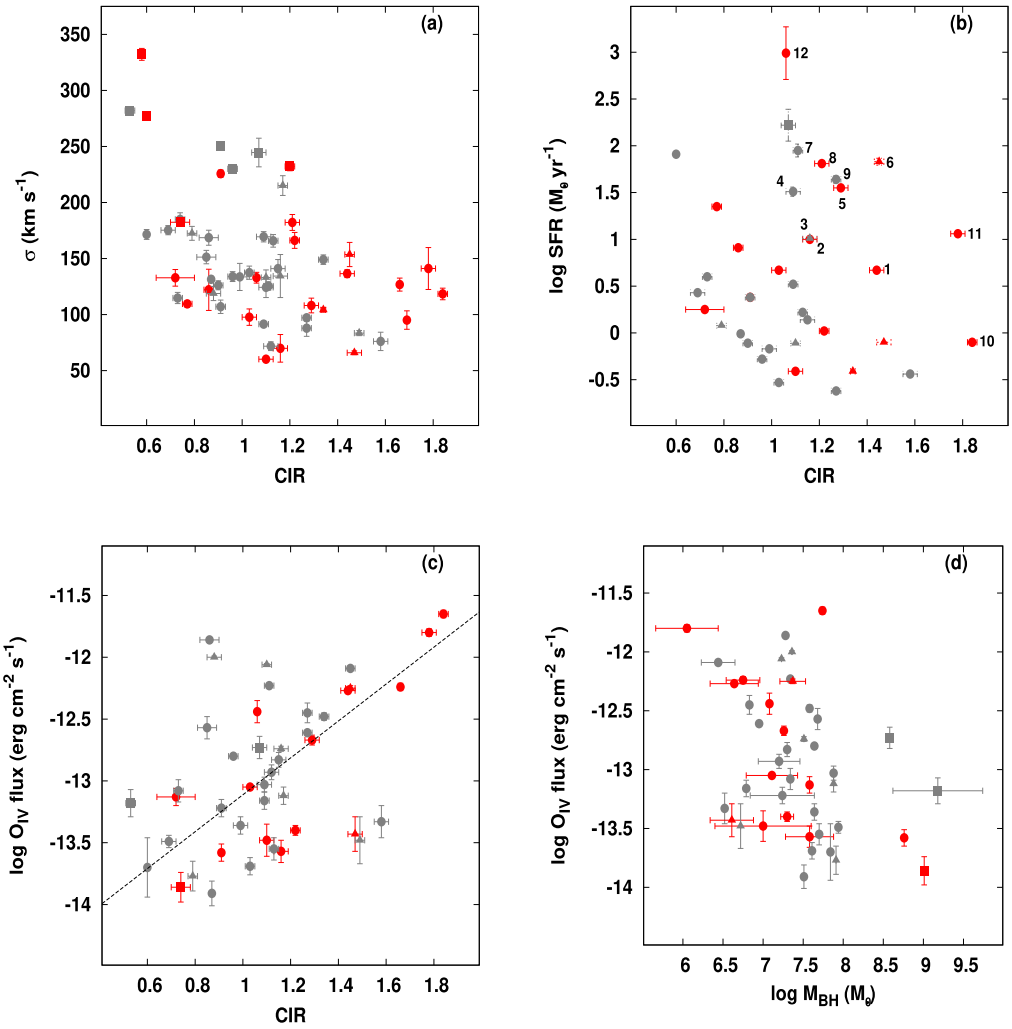

Figure 2. Variations between the CIR and (a) stellar velocity dispersion adopted from HyperLEDA database, (b) circumnuclear SFR, (c) O IV flux of AGN and (d) the inter-connection between $M_{\rm BH}$ and O IV flux of the sample galaxies. O IV flux values are taken from Diamond-Stanic et al. (2009). The symbols used to represent the galaxies are same as those in Figure 1.

3.3. Variation between the CIR and SFR

In Figure 2(b), we explore the connection between CIR and circumnuclear SFR traced by the UV luminosity (FUV) in an aperture of radius 10″ at the galactic center. We find that there is no correlation between CIR and circumnuclear SFR. The properties of sub-structures in the nuclear region of host galaxies may influence the star formation process, thereby affecting CIR. The galaxies IC 2560, NGC 0788, NGC 1667, NGC 3516, NGC 5427 and NGC 6814, denoted by numbers 1 to 6 respectively in the figure, possess nuclear dust spirals, which can regulate the nuclear SFR at the central region of the galaxies (Evans et al. 1996; Pérez-Ramírez et al. 2000; Martini et al. 2003; Muñoz Marín et al. 2007). The galaxies IC 3639, NGC 2782, NGC 5135 and NGC 7582, numbered 7 to 10, with nuclear starburst activity (Boer et al. 1992; González Delgado et al. 2001; Muñoz Marín et al. 2007; Bianchi et al. 2007) are also apparent outliers in the figure. NGC 1365 and NGC 7469 are the galaxies showing intense nuclear SFR, with star-forming regions concentrated in hot spots around the nucleus (Davies et al. 2007; Ramos Almeida et al. 2009), which are displayed in the figure by the numbers 11 and 12 respectively. By excluding these galaxies, we may see a negative trend in CIR and SFR. However, it is insufficient to confirm any connection between CIR and SFR, necessitating a thorough investigation with larger sample size.

3.4. Variation Between the CIR and O IV Flux

In Figure 2(c), we show the observed correlation between CIR and O IV flux of the host galaxy, which is taken from Diamond-Stanic et al. (2009). O IV flux is an accurate measure

Table 2
The Table Lists the Best-fitting Parameters for the Relation $x = \alpha$ CIR + β and Correlation Coefficients for Various Relations

x	α	β	r	s	n
log M_{BH} (spiral+lenticular)	-1.25 ± 0.16	8.67 ± 0.19	-0.74	>99.99%	47
log M_{BH} (elliptical)	-1.16 ± 0.15	9.67 ± 0.13	-0.94	99.40%	8
log O IV flux	1.49 ± 0.24	-14.60 ± 0.28	0.70	>99.99%	38

of intrinsic AGN luminosity (Diamond-Stanic et al. 2009) and we find a positive correlation with CIR ($r = 0.70$ with $s > 99.99\%$). O IV emission (25.9 μm) is a tracer of highly ionized gas of the order of 35–97 eV, and these types of mid-infrared emission lines can be produced in the vicinity of hot stars in the central region of AGN host galaxies (Pottasch et al. 2001; Smith et al. 2004; Devost 2007). AGN luminosity depends upon the fuel consumed by the SMBH at the nuclear region of the galaxy, and ETGs have less fuel than LTGs (Rieke 2002). This suggests that AGN power is likely to decrease while SMBH grows in the host galaxy. However, NGC 3081, NGC 3185, NGC 3281, NGC 5273 and NGC 7743 deviated from this correlation.

4. Discussion and Conclusion

We report photometric analysis of Seyfert galaxies using the recently discovered parameter CIR. The CIR shows good correlations with many structural parameters of host galaxies, especially with the mass of the SMBHs residing at the centers of galaxies (Aswathy & Ravikumar 2018, 2020). For Seyfert galaxies also, the CIR shows strong anti-correlation with the mass of SMBHs. However, the massive SMBHs hosted by ellipticals in the sample display a distinctive trend from that displayed by lenticulars and spirals, in the sense that ellipticals host more massive SMBHs than those hosted by lenticulars and spirals. The disky systems are indistinguishable in the correlation. It is possible that the more massive the central SMBH, the higher the suppression of star formation due to feedback (Harrison 2017). As a decrease in the light in the inner aperture reduces the value of CIR, we can expect the anti-correlation between CIR and mass of SMBH.

The AGN feedback mechanism has a significant role in the evolution process of galaxies, in which the energy released by an AGN to the surrounding galactic medium halts the cooling of gas in the central region of galaxies and also removes the gas in the form of massive outflows (Morganti 2017). The AGN feedback process is considered to be a key factor of galaxy evolution and has been included in several simulations and analytical models for years (e.g., Kauffmann & Haehnelt 2000; Di Matteo et al. 2005; Schaye et al. 2015; Sijacki et al. 2015). This feedback may suppress star formation at the central part of the galaxy and may decrease or stall completely the growth of the SMBH (e.g., Croton et al. 2006; Sijacki et al. 2007), thus setting up a co-evolution scenario for the galaxy and its SMBH (Aswathy & Ravikumar 2018). Around 30% of Seyfert galaxies are reported to possess outflow incidents (Crenshaw et al. 2003; Crenshaw & Kraemer 2007; Crenshaw et al. 2012). The pc scale AGN-driven outflows in the massive galaxies can expel the gas from the nuclear region, which may reduce the gas accretion toward the center of the galaxy and lead to quenching of star formation at the central region (Morganti 2017). This interesting phenomenon has been observed in optical, UV and X-ray emissions, and could be traced to such outflows using ionized gas and absorption lines (e.g., Veilleux et al. 2005; Bland-Hawthorn et al. 2007; Tadhunter 2008; King & Pounds 2015).

Different studies argued for the probability of AGN feedback by a thermal process in the vicinity of the SMBH (e.g., Di Matteo et al. 2005; Springel et al. 2005; Johansson et al. 2009). Simulations of the AGN feedback mechanism suggest that the Compton heating effect can raise the temperature of the the gas at the nuclear region, about 10–35 pc, to $\sim 10^9$ K (e.g., Gan et al. 2014; Melioli & de Gouveia Dal Pino 2015). This AGN heating may also reduce star formation in the central region of the galaxy, and thus the value of CIR.

Stellar velocity dispersion (σ) of the bulge component is strongly connected with the central SMBH (Ferrarese & Merritt 2000; Gebhardt et al. 2000; Tremaine et al. 2002; Gültekin et al. 2009). Active galaxies also obey the $\sigma - M_{BH}$ relation, but with significant scatter (Caglar et al. 2020). It is also reported that CIR of ETGs is well correlated with the stellar velocity dispersion (Aswathy & Ravikumar 2018). In the present study, however, Seyfert galaxies show a large scatter in the CIR-σ relation, even though there is a strong CIR - M_{BH} relation. The uncertainties present in the measurement of stellar velocity dispersion could be high when excessively illuminated by the central AGN (Riffel et al. 2013). Furthermore, stellar velocity dispersion measurements may be skewed due to the rotational effect of stellar disks (Woo et al. 2015). In order to explain this further, we have plotted the variation of M_{BH} with σ in Figure 3. The velocity dispersion measurements for galaxies with dynamical estimation of mass of the SMBH available, shown in red, clearly display a larger scatter than those of galaxies without dynamical estimation of M_{BH} (gray points). For the $\sigma - M_{BH}$ correlation in the combined sample of spirals and lenticulars, we obtained a linear correlation

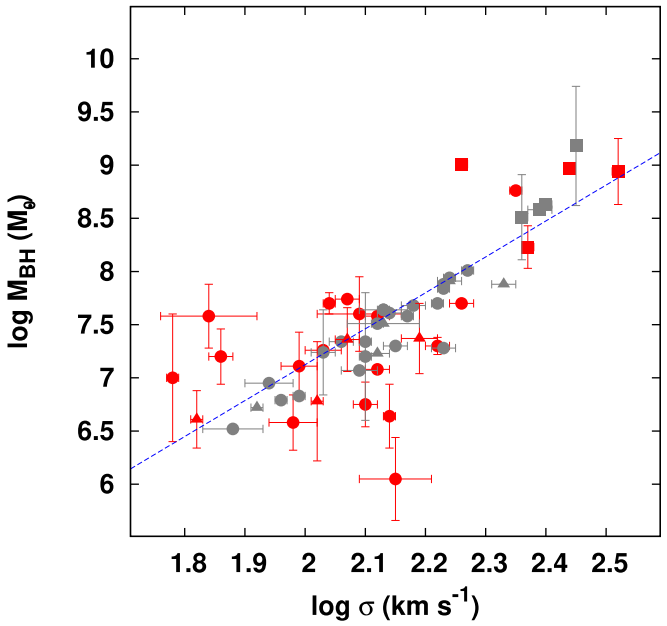

Figure 3. Variation between stellar velocity dispersion and mass of the SMBH of sample galaxies along with the best fit adopted from Caglar et al. (2020). The symbols used to represent the galaxies are the same as those in Figure 1.

coefficient of $r = 0.65$ with significance $s > 99.99\%$. At the same time, the correlation coefficient of the CIR - $M_{\rm BH}$ (for spirals + lenticulars) relation is $r = -0.74$ with significance $s > 99.99\%$. The scatters of the correlations $\sigma - M_{\rm BH}$ and CIR-$M_{\rm BH}$ are 2.63 and 2.04 dex respectively, further establishing that the CIR is, in fact, a better tracer of the $M_{\rm BH}$ than the central velocity dispersion.

The observed correlation between CIR and O IV flux, shown in Figure 2(c), also displays the possibility of larger uncertainties present in measurement of emission lines in galaxies associated with AGNs (e.g., Lutz et al. 2003; Armus et al. 2006, 2007; Diamond-Stanic et al. 2009; Veilleux et al. 2009). In this case also, the correlation coefficient increases to 0.76 with a significance of $s = 99.38\%$ if we just consider galaxies with dynamically estimated SMBH masses, but it drops to 0.62 ($s = 99.74\%$) when these data points are excluded. Seyfert galaxies with high O IV flux emission possess enhanced nuclear star formation (Diamond-Stanic & Rieke 2012), and an increase in CIR is expected in galaxies with increased O IV emission. However, the O IV flux of the sample galaxies shows only a weak anti-correlation ($r = -0.58$ with $s = 99.95\%$) with the mass of SMBH shown in Figure 2(d), possibly due to the increased uncertainties involved in both the quantities.

Generally, Seyfert galaxies can be observed and located through the UV emission coming out from the sources (Rieke 2002). Apart from age and morphological classification, the common feature of Seyfert galaxies is their intense star formation (Cid Fernandes et al. 2004; Davies et al. 2007; Sarzi et al. 2007; Kauffmann & Heckman 2009). We explore the variation of the estimated circumnuclear SFR by the excess UV with CIR, as depicted in Figure 2(b). We notice that the galaxies harboring central structures such as pc scale nuclear dust spiral, nuclear starburst and the galaxies possessing high SFR exhibit large deviation in the observed CIR – SFR relation. The measure of nuclear SFR has been shown to increase from the central region to the outskirts of galaxies (Diamond-Stanic & Rieke 2012; Esquej et al. 2014). The outflow from the central part of the galaxy due to the AGN feedback mechanism can interact with the interstellar medium (ISM) effectively (Ostriker et al. 2010; Weinberger et al. 2017; Yuan et al. 2018). The feedback-driven outflow of gas enhances the star formation at larger radii from the core of the galaxy (Ishibashi et al. 2013; Ishibashi & Fabian 2014). This outflow of gas can be responsible for enhancing the circumnuclear SFR. All these can affect measurements of both SFR and CIR, rendering a weak correlation between the two.

We employed CIR to explore the presence of central features in Seyfert galaxies and their role in galaxy evolution. The analysis shows that CIR measured for Seyfert galaxies predicts the mass of central SMBHs even better than the estimates obtained by spectroscopic parameters like the central velocity dispersion. Being a photometric tool, this promises a cheap and fast technique to explore large galaxy samples, which has great potential in observations of new generation facilities like the James Webb Space Telescope.

Acknowledgments

We sincerely thank the anonymous referee for her/his comments which improved the quality of the paper significantly. V.K.T. would like to acknowledge the financial support from the Council of Scientific & Industrial Research (CSIR), Government of India. We acknowledge the use of the NASA/IPAC Extragalactic Database (NED), https://ned.ipac.caltech.edu/ operated by the Jet Propulsion Laboratory, California Institute of Technology, and the Hyperleda database, http://leda.univ-lyon1.fr/. We acknowledge the use of data publicly available at the Mikulski Archive for Space Telescopes (MAST), http://archive.stsci.edu/ observed by the NASA/ESA Hubble Space Telescope and Galaxy Evolution Explorer (GALEX) led by the California Institute of Technology http://galex.stsci.edu/.

References

Abraham, R. G., Valdes, F., Yee, H. K. C., & van den Bergh, S. 1994, ApJ, 432, 75
Alatalo, K., Lacy, M., Lanz, L., et al. 2015, ApJ, 798, 31
Alexander, D., & Hickox, R. 2012, NewAR, 56, 93
Alonso-Herrero, A., Pereira-Santaella, M., Rieke, G. H., et al. 2013, ApJ, 765, 78
Armus, L., Bernard-Salas, J., Spoon, H. W. W., et al. 2006, ApJ, 640, 204

Armus, L., Charmandaris, V., Bernard-Salas, J., et al. 2007, ApJ, 656, 148
Aswathy, S., & Ravikumar, C. D. 2018, MNRAS, 477, 2399
Aswathy, S., & Ravikumar, C. D. 2020, RAA, 20, 015
Barth, A. J., Ho, L. C., Filippenko, A. V., Rix, H.-W., & Sargent, W. L. W. 2001, ApJ, 546, 205
Beifiori, A., Courteau, S., Corsini, E. M., & Zhu, Y. 2012, MNRAS, 419, 2497
Bertin, E., & Arnouts, S. 1996, A&As, 117, 393
Bianchi, S., Chiaberge, M., Piconcelli, E., & Guainazzi, M. 2007, MNRAS, 374, 697
Bland-Hawthorn, J., Veilleux, S., & Cecil, G. 2007, Ap&SS, 311, 87
Boer, B., Schulz, H., & Keel, W. C. 1992, A&A, 260, 67
Busch, G., Eckart, A., Valencia-S, M., et al. 2017, A&A, 598, A55
Caglar, T., Burtscher, L., Brandl, B., et al. 2020, A&A, 634, A114
Christensen, L., Jahnke, K., Wisotzki, L., et al. 2006, A&A, 452, 869
Cid Fernandes, R., Gu, Q., Melnick, J., et al. 2004, MNRAS, 355, 273
Cid Fernandes, R., Heckman, T., Schmitt, H., González Delgado, R. M., & Storchi-Bergmann, T. 2001, ApJ, 558, 81
Cid Fernandes, Roberto, J., & Terlevich, R. 1995, MNRAS, 272, 423
Cid-Fernandes, R., Schmitt, H. R., & Storchi-Bergmann, T. 2001, RMxAA, 11, 133
Combes, F., García-Burillo, S., Audibert, A., et al. 2019, A&A, 623, A79
Conselice, C. J. 2003, ApJS, 147, 1
Crenshaw, D. M., Fischer, T. C., Kraemer, S. B., Schmitt, H. R., & Turner, T. J. 2012, in ASP Conf. Ser. 460, AGN Winds in Charleston, ed. G. Chartas, F. Hamann, & K. M. Leighly (San Francisco, CA: ASP), 261
Crenshaw, D. M., & Kraemer, S. B. 2007, in ASP Conf. Ser. 373, The Central Engine of Active Galactic Nuclei, ed. L. C. Ho & J. W. Wang (San Francisco, CA: ASP), 319
Crenshaw, D. M., Kraemer, S. B., & George, I. M. 2003, ARA&A, 41 117
Croton, D. J., Springel, V., White, S. D. M., et al. 2006, MNRAS, 365, 11
Davies, R. I., Müller Sánchez, F., Genzel, R., et al. 2007, ApJ, 671, 1388
Davis, B. L., Berrier, J. C., Johns, L., et al. 2014, ApJ, 789, 124
Davis, B. L., Graham, A. W., & Cameron, E. 2018, ApJ, 869, 113
Davis, B. L., Graham, A. W., & Cameron, E. 2019, ApJ, 873, 85
de Vaucouleurs, G., de Vaucouleurs, A., de Vaucouleurs, H. G., Jr, et al. 1991, Third Reference Catalogue of Bright Galaxies (New York: Springer)
Devost, D. 2007, AAS Meeting Abstracts, 210, 112.09
Di Matteo, T., Springel, V., & Hernquist, L. 2005, Natur, 433, 604
Diamond-Stanic, A. M., & Rieke, G. H. 2012, ApJ, 746, 168
Diamond-Stanic, A. M., Rieke, G. H., & Rigby, J. R. 2009, ApJ, 698, 623
Dong, A.-J., & Wu, Q. 2015, MNRAS, 453, 3447
Dong, X. Y., & De Robertis, M. M. 2006, AJ, 131, 1236
Dullo, B. T., Knapen, J. H., Williams, D. R. A., et al. 2018, MNRAS, 475, 4670
Dumas, G., Mundell, C. G., Emsellem, E., & Nagar, N. M. 2007, MNRAS, 379, 1249
Ellison, S. L., Patton, D. R., Mendel, J. T., & Scudder, J. M. 2011, MNRAS, 418, 2043
Esquej, P., Alonso-Herrero, A., González-Martín, O., et al. 2014, ApJ, 780, 86
Evans, I. N., Koratkar, A. P., Storchi-Bergmann, T., et al. 1996, ApJS, 105, 93
Ferrarese, L., & Merritt, D. 2000, ApJL, 539, L9
Gadotti, D. A., & Sánchez-Janssen, R. 2012, MNRAS, 423, 877
Gan, Z., Yuan, F., Ostriker, J. P., Ciotti, L., & Novak, G. S. 2014, ApJ, 789, 150
García-Burillo, S., Combes, F., Usero, A., et al. 2014, A&A, 567, A125
Gebhardt, K., Bender, R., Bower, G., et al. 2000, ApJL, 539, L13
Gil de Paz, A., Madore, B. F., Boissier, S., et al. 2005, ApJL, 627, L29
Gil de Paz, A., Madore, B. F., Boissier, S., et al. 2007, ApJ, 661, 115
González Delgado, R. M., Heckman, T., & Leitherer, C. 2001, ApJ, 546, 845
Goulding, A. D., Alexander, D. M., Lehmer, B. D., & Mullaney, J. R. 2010, MNRAS, 406, 597
Graham, A. W., & Soria, R. 2019, MNRAS, 484, 794
Gültekin, K., Richstone, D. O., Gebhardt, K., et al. 2009, ApJ, 698, 198
Häring, N., & Rix, H.-W. 2004, ApJL, 604, L89
Harrison, C. M. 2017, NatAs, 1, 0165
Heckman, T. M., & Best, P. N. 2014, ARA&A, 52, 589
Ho, L. C. 2008, ARA&A, 46, 475
Ho, L. C., Filippenko, A. V., & Sargent, W. L. 1995, ApJS, 98, 477
Hopkins, P. F., Hernquist, L., Cox, T. J., et al. 2006, ApJS, 163, 1
Hopkins, P. F., Torrey, P., Faucher-Giguère, C.-A., Quataert, E., & Murray, N. 2016, MNRAS, 458, 816
Ishibashi, W., & Fabian, A. C. 2014, MNRAS, 441, 1474
Ishibashi, W., Fabian, A. C., & Canning, R. E. A. 2013, MNRAS, 431, 2350
Izumi, T., Kawakatu, N., & Kohno, K. 2016, ApJ, 827, 81
Johansson, P. H., Naab, T., & Burkert, A. 2009, ApJ, 690, 802
Kauffmann, G., & Haehnelt, M. 2000, MNRAS, 311, 576
Kauffmann, G., & Heckman, T. M. 2009, MNRAS, 397, 135
Kauffmann, G., Heckman, T. M., Tremonti, C., et al. 2003, MNRAS, 346, 1055
Kawakatu, N., Anabuki, N., Nagao, T., Umemura, M., & Nakagawa, T. 2006, ApJ, 637, 104
King, A., & Pounds, K. 2015, ARA&A, 53, 115
Koliopanos, F., Ciambur, B. C., Graham, A. W., et al. 2017, A&A, 601, A20
Koribalski, B. S., & López-Sánchez, Á. R. 2009, MNRAS, 400, 1749
Kormendy, J., & Ho, L. C. 2013, ARA&A, 51, 511
Kormendy, J., & Richstone, D. 1995, ARA&A, 33, 581
Krause, M., Fendt, C., & Neininger, N. 2007, A&A, 467, 1037
López-Sánchez, Á. R. 2010, A&A, 521, A63
Lutz, D., Sturm, E., Genzel, R., et al. 2003, A&A, 409, 867
Magorrian, J., Tremaine, S., Richstone, D., et al. 1998, AJ, 115, 2285
Maiolino, R., Krabbe, A., Thatte, N., & Genzel, R. 1998, ApJ, 493, 650
Marconi, A., & Hunt, L. K. 2003, ApJL, 589, L21
Martini, P., Regan, M. W., Mulchaey, J. S., & Pogge, R. W. 2003, ApJ, 589, 774
McConnell, N. J., & Ma, C.-P. 2013, ApJ, 764, 184
Melioli, C., & de Gouveia Dal Pino, E. M. 2015, ApJ, 812, 90
Morganti, R. 2017, FrASS, 4, 42
Morganti, R., Oosterloo, T., Oonk, J. B. R., Frieswijk, W., & Tadhunter, C. 2015, A&A, 580, A1
Muñoz Marín, V. M., González Delgado, R. M., Schmitt, H. R., et al. 2007, AJ, 134, 648
Nowak, N., Thomas, J., Erwin, P., et al. 2010, MNRAS, 403, 646
Onken, C. A., Peterson, B. M., Dietrich, M., Robinson, A., & Salamanca, I. M. 2003, ApJ, 585, 121
Osterbrock, D. E., & Martel, A. 1993, ApJ, 414, 552
Ostriker, J. P., Choi, E., Ciotti, L., Novak, G. S., & Proga, D. 2010, ApJ, 722, 642
Pellegrini, S. 2010, ApJ, 717, 640
Pérez-Ramírez, D., Knapen, J. H., Peletier, R. F., et al. 2000, MNRAS, 317, 234
Pottasch, S. R., Beintema, D. A., Bernard Salas, J., & Feibelman, W. A. 2001, A&A, 380, 684
Pović, M., Sánchez-Portal, M., Pérez García, A. M., et al. 2009, ApJ, 706, 810
Press, W. H., Teukolsky, S. A., Vetterling, W. T., & Flannery, B. P. 1992, Numerical Recipes in FORTRAN. The Art of Scientific Computing (Cambridge: Cambridge Univ. Press)
Querejeta, M., Schinnerer, E., García-Burillo, S., et al. 2016, A&A, 593, A118
Ramos Almeida, C., Levenson, N. A., Rodríguez Espinosa, J. M., et al. 2009, ApJ, 702, 1127
Rashed, Y. E., Eckart, A., Eckart, A., et al. 2015, MNRAS, 454, 2918
Rieke, G. H. 2002, in ASP Conf. Ser. 258, Issues in Unification of Active Galactic Nuclei, ed. R. Maiolino, A. Marconi, & N. Nagar (San Francisco, CA: ASP), 113
Riffel, R. A., Storchi-Bergmann, T., Dors, O. L., & Winge, C. 2009, MNRAS, 393, 783
Riffel, R. A., Storchi-Bergmann, T., Riffel, R., et al. 2013, MNRAS, 429, 2587
Salim, S., Rich, R. M., Charlot, S., et al. 2007, ApJS, 173, 267
Sandage, A., & Tammann, G. A. 1987, A Revised Shapley-Ames Catalog of Bright Galaxies
Sarzi, M., Allard, E. L., Knapen, J. H., & Mazzuca, L. M. 2007, MNRAS, 380, 949
Savorgnan, G. A. D., & Graham, A. W. 2015, MNRAS, 446, 2330
Savorgnan, G. A. D., & Graham, A. W. 2016, ApJS, 222, 10
Schaye, J., Crain, R. A., Bower, R. G., et al. 2015, MNRAS, 446, 521
Shapley, H., & Ames, A. 1932, AnHar, 88, 41
Sijacki, D., Springel, V., Di Matteo, T., & Hernquist, L. 2007, MNRAS, 380, 877
Sijacki, D., Vogelsberger, M., Genel, S., et al. 2015, MNRAS, 452, 575
Silverman, J. D., Kampczyk, P., Jahnke, K., et al. 2011, ApJ, 743, 2

Smajić, S., Moser, L., Eckart, A., et al. 2014, A&A, 567, A119
Smith, J. D. T., Dale, D. A., Armus, L., et al. 2004, ApJS, 154, 199
Springel, V., Di Matteo, T., & Hernquist, L. 2005, MNRAS, 361, 776
Sruthi, K., & Ravikumar, C. D. 2021, MNRAS, 500, 1343
Tadhunter, C. 2008, MmSAI, 79, 1205
Terlevich, R., & Melnick, J. 1985, MNRAS, 213, 841
Thilker, D. A., Bianchi, L., Boissier, S., et al. 2005, ApJL, 619, L79
Tremaine, S., Gebhardt, K., Bender, R., et al. 2002, ApJ, 574, 740
van den Bosch, R. C. E. 2016, ApJ, 831, 134
Veilleux, S., Cecil, G., & Bland-Hawthorn, J. 2005, ARA&A, 43, 769
Veilleux, S., Rupke, D. S. N., Kim, D. C., et al. 2009, ApJS, 182, 628
Villforth, C., Sarajedini, V., & Koekemoer, A. 2012, MNRAS, 426, 360
Wang, J., Fabbiano, G., Karovska, M., Elvis, M., & Risaliti, G. 2012, ApJ, 756, 180
Weedman, D. W. 1977, ARA&A, 15, 69
Weinberger, R., Springel, V., Hernquist, L., et al. 2017, MNRAS, 465, 3291
Woo, J.-H., Yoon, Y., Park, S., Park, D., & Kim, S. C. 2015, ApJ, 801, 38
Wylezalek, D., & Zakamska, N. L. 2016, MNRAS, 461, 3724
Yuan, F., Yoon, D., Li, Y.-P., et al. 2018, ApJ, 857, 121